Revisiting $K_1(1270) - K_1(1400)$ mixing with QCD sum rules

Yu-Ji Shi,[1,2,†] Jun Zeng,[2,*] and Zhi-Fu Deng[2]

[1]*School of Physics, East China University of Science and Technology, Shanghai 200237, China*
[2]*INPAC, Key Laboratory for Particle Astrophysics and Cosmology (MOE), Shanghai Key Laboratory for Particle Physics and Cosmology, School of Physics and Astronomy, Shanghai Jiao Tong University, Shanghai 200240, China*

(Received 6 November 2023; revised 12 December 2023; accepted 2 January 2024; published 30 January 2024)

We investigate the $K_1(1270) - K_1(1400)$ mixing induced by the flavor $SU(3)$ symmetry breaking. The mixing angle is calculated in a purely theoretical manner, where it is expressed by a $K_{1A} \to K_{1B}$ transition matrix element of the operators that break flavor $SU(3)$ symmetry. The QCD contribution to this matrix element is assumed to be dominated and calculated with QCD sum rules. A three-point correlation function is defined and handled both at the hadron and quark-gluon levels. The quark-gluon level calculation is based on operator product expansion up to dimension-five condensates. A detailed numerical analysis is performed to determine the Borel parameters, and the obtained mixing angle is $\theta_{K_1} = 21.4° \pm 9°$ or $\theta_{K_1} = 68.6° \pm 9°$.

DOI: 10.1103/PhysRevD.109.016027

I. INTRODUCTION

The flavor $SU(3)$ symmetry plays an important role in the conventional quark model, which classifies hadrons into various irreducible representations. Although the assumption of perfect flavor $SU(3)$ symmetry succeeds in most phenomenological analyses of hadron decays and spectrums [1–8], its breaking effect still cannot be neglected. One of the physical effects due to flavor $SU(3)$ breaking is the hadron mixing.

According to the quark model, the two axial-vector nonets with $J^P = 1^+$ are expected as the orbital excitation of the $\bar{q}q$ system. There are two types of P-wave axial-vector mesons: $^3P_1$ and $^1P_1$ with the notation $^{2S+1}L_J$. Generally, in the flavor $SU(3)$ limit, these two nonets cannot be mixed since they have distinct C parities, explicitly, $J^{PC} = 1^{++}, 1^{+-}$ for $^3P_1$, $^1P_1$ respectively. However, because of the mass difference between the strange and light quarks, the kaon nonets $K_{1A}(^3P_1)$ and $K_{1B}(^1P_1)$ are distinguished from the mass eigenstates $K_1(1270)$ and $K_1(1400)$. As a result, there emerges a mixing between these two sets of axial-vector kaons,

$$\begin{pmatrix} |K_1(1270)\rangle \\ |K_1(1400)\rangle \end{pmatrix} = \begin{pmatrix} \cos\theta_{K_1} & \sin\theta_{K_1} \\ -\sin\theta_{K_1} & \cos\theta_{K_1} \end{pmatrix} \begin{pmatrix} |K_{1B}\rangle \\ |K_{1A}\rangle \end{pmatrix}, \quad (1)$$

where θ_{K_1} is the mixing angle. θ_{K_1} is an crucial input parameter in the studies of exotic B meson decays $B \to K_1 l^+ l^-$, which provides an ideal platform for searching new physics [9–19].

Up to now, there have been quite a number of theoretical studies on θ_{K_1} in the literature, with most of them based on phenomenological analysis. An indirect method of measuring θ_{K_1} in D meson decays was proposed in Ref. [20]. An approach to extract the mixing angle from the ratios of partial wave amplitudes can be found in Ref. [21]. In Ref. [22], with the use of early experimental information on masses and the partial rates of $K_1(1270)$ and $K_1(1400)$, the authors obtained $\theta_{K_1} = 33°$ or $57°$; Refs. [23,24] phenomenologically analyzed the $\tau \to K_1(1270)\nu_\tau$ and $\tau \to K_1(1400)\nu_\tau$ decays and obtained $\theta_{K_1} = 37°$ or $58°$; Ref. [25] studied the correlation of the $f_1(1285) - f_1(1420)$ mixing angle $\theta_{^3P_1}$ with θ_{K_1}, and obtained $\theta_{K_1} = 31.7°$ or $56.3°$. In Ref. [26], the authors used the correspondence between θ_{K_1} and the $f_1(1285) - f_1(1420)$, $h_1(1170) - h_1(1380)$ mixing angles to rule out unreasonable θ_{K_1} values and announced a reasonable range as $28° < \theta_{K_1} < 30°$.

In addition to the pure phenomenological analysis mentioned above, there are also studies on θ_{K_1} referring to both phenomenological inputs and theoretical calculations. In Ref. [27], the authors obtained $34° < \theta_{K_1} < 55°$ with the nonrelativistic constituent quark model with inputs of the mass difference between the $a_1(1260)$ and $b_1(1235)$ mesons, as well as the ratio of the constituent quark masses. In Ref. [28], $\theta_{K_1} = 33°$ and $58°$ were obtained by perturbative QCD (pQCD) calculation referring to the $B \to J/\psi K_1(1270)$, $J/\psi K_1(1400)$ decays. Furthermore, a pure theoretical prediction of θ_{K_1} was given with QCD sum rules (QCDSRs) in Ref. [29]. The authors related θ_{K_1} with a two-point

*Corresponding author: zengj@sjtu.edu.cn
†Corresponding author: shiyuji@ecust.edu.cn

correlation function, which is calculated with operator product expansion and they obtained $\theta_{K_1} = 39° \pm 4°$. However, this QCDSR calculation is not perfect due to the missing pseudoscalar kaon contribution at the hadron level.

In this work, we perform a purely theoretical calculation of θ_{K_1}, which is independent of various decays referring to $K_1(1270)$ and $K_1(1400)$. The θ_{K_1} can be extracted from a $K_{1A} \to K_{1B}$ transition matrix element induced by $SU(3)$ breaking operators, with zero transferring momentum. This method has been successfully applied to the studies of $\Xi_c - \Xi_c'$ mixing [30,31]. The $SU(3)$ breaking transition matrix element is calculated with QCDSRs with a three-point correlation function, a different method from that used in Ref. [29]. Some introductions to QCDSRs and their applications can be found in Refs. [32–39,40].

This paper is arranged as follows: In Sec. II, we introduce the method to extract θ_{K_1}. Section III gives the hadron level calculation, and Sec. IV gives the quark-gluon level calculation. Section V presents numerical results. Section VI is a summary of this work.

II. $K_1(1270) - K_1(1400)$ MIXING

There are two sources of the flavor $SU(3)$ breaking. The first one comes from the mass difference between s and u, d (nearly massless) quarks, which only provides QCD contribution to $K_1(1270) - K_1(1400)$ mixing. Another source comes from the electric charge difference among the u, d, s quarks, which involves the QED effect. In this work, we will focus on the QCD contribution since the QED effect is expected to be tiny, as shown by our previous work on the $\Xi_c - \Xi_c'$ mixing [30,31]. The full QCD Lagrangian of the quark sector contains both the terms conserving and breaking the flavor $SU(3)$ symmetry: $\mathcal{L}_{\rm QCD} = \mathcal{L}_0 + \Delta\mathcal{L}$, where $\mathcal{L}_0$ reads as

$$\mathcal{L}_0 = \sum_q \bar{q}(iD - m_u)q, \tag{2}$$

with D being the QCD covariant derivative, $q = u$, d, s, and $m_u = m_d = 0$ is approximately assumed. The $SU(3)$ symmetry breaking term $\Delta\mathcal{L}$, which arises from the quark mass difference, reads as

$$\Delta\mathcal{L} = \bar{s}(m_u - m_s)s. \tag{3}$$

Accordingly, the Hamiltonian is decomposed as $H = H_0 + \Delta H$, with

$$\Delta H = \int d^3x \Delta\mathcal{H}(x) = -\int d^3x \Delta\mathcal{L}(x). \tag{4}$$

The lowest axial-vector kaons $K_1(1270)$ and $K_1(1400)$ are the mass eigenstates of the full Hamiltonian H,

$$H|K_1(1270)\rangle = m_{1270}|K_1(1270)\rangle,$$
$$H|K_1(1400)\rangle = m_{1400}|K_1(1270)\rangle. \tag{5}$$

On the other hand, in the $SU(3)$ symmetry limit, the lowest axial-vector kaons are classified into $K_{1B}(^1P_1)$ and $K_{1A}(^3P_1)$ states, which are eigenstates of the $SU(3)$ conserved Hamiltonian H_0,

$$H_0|K_{1B}\rangle = m_{1B}|K_{1B}\rangle,$$
$$H_0|K_{1A}\rangle = m_{1A}|K_{1A}\rangle. \tag{6}$$

The mixing between the physical doublet $|K_P\rangle = (|K_1(1270)\rangle, |K_1(1400)\rangle)^T$ and the $SU(3)$ doublet $|K_F\rangle = (|K_{1B}\rangle, |K_{1A}\rangle)^T$ is described by a unitary transforming matrix U with a mixing angle θ_{K_1},

$$|K_P\rangle = \begin{pmatrix} \cos\theta_{K_1} & \sin\theta_{K_1} \\ -\sin\theta_{K_1} & \cos\theta_{K_1} \end{pmatrix}|K_F\rangle = U|K_F\rangle. \tag{7}$$

Here we consider the matrix element for the $SU(3)$ doublet $|K_F\rangle$: $\langle K_F(p')|H|K_F(p)\rangle$. Both the initial and final states are set to be static $\vec{p} = \vec{p}' = 0$ and on shell $p^0_{1B} = m_{1B}$, $p^0_{1A} = m_{1A}$. With the use of the unitary transformation U defined in Eq. (7) and the physical masses defined in Eq. (5), we obtain

$$\begin{pmatrix} \langle K_{1B}(\lambda')|H|K_{1B}(\lambda)\rangle & \langle K_{1B}(\lambda')|H|K_{1A}(\lambda)\rangle \\ \langle K_{1A}(\lambda')|H|K_{1B}(\lambda)\rangle & \langle K_{1A}(\lambda')|H|K_{1A}(\lambda)\rangle \end{pmatrix}$$
$$= 2(2\pi)^3\delta^{(3)}(\vec{0})\delta_{\lambda\lambda'}$$
$$\times \begin{pmatrix} m^2_{1270}c_k^2 + m^2_{1400}s_k^2 & (m^2_{1270} - m^2_{1400})c_k s_k \\ (m^2_{1270} - m^2_{1400})c_k s_k & m^2_{1270}s_k^2 + m^2_{1400}c_k^2 \end{pmatrix}, \tag{8}$$

where $s_k = \sin\theta_{K_1}$ and $c_k = \cos\theta_{K_1}$. For simplicity, the momentum dependence of the $K_{1B,1A}$ states are not shown in the matrix element.

It can be found that the upper-right off-diagonal component in Eq. (8) leads to the equation

$$\langle K_{1B}(\lambda')|H|K_{1A}(\lambda)\rangle$$
$$= (2\pi)^3\delta^{(3)}(\vec{0})\delta_{\lambda\lambda'}(m^2_{1270} - m^2_{1400})\sin 2\theta_{K_1}. \tag{9}$$

Therefore, the mixing angle θ_{K_1} can be extracted as soon as one calculates the matrix element on the left-hand side above, which can be further expressed as

$$\langle K_{1B}(\lambda')|H|K_{1A}(\lambda)\rangle$$
$$= (2\pi)^3\delta^{(3)}(\vec{0})\langle K_{1B}(\lambda')|\Delta\mathcal{H}(0)|K_{1A}(\lambda)\rangle, \tag{10}$$

by integrating out the coordinate. Equating Eqs. (9) and (10), and setting $\lambda = \lambda'$, we have

$$\sin 2\theta_{K_1} = \frac{m_s - m_u}{m^2_{1270} - m^2_{1400}}\langle K_{1B}|\bar{s}s(0)|K_{1A}\rangle. \tag{11}$$

Generally, the matrix element $\langle K_{1B}(p_2)|\Delta\mathcal{H}(0)|K_{1A}(p_1)\rangle$ with nonzero initial and final momentums can be parametrized as

$$\langle K_{1B}(p_2)|\bar{s}s(0)|K_{1A}(p_1)\rangle = \epsilon_\mu^*(p_2)\left[F_1 g^{\mu\nu} + \frac{F_2}{M^2}\epsilon^{\mu\nu\alpha\beta}p_{1\alpha}p_{2\beta} + \frac{F_3}{M^2}p_1^\mu p_2^\nu\right]\epsilon_\nu(p_1), \tag{12}$$

where $F_{1,2,3}$ are three transition functions of $q^2 = (p_1 - p_2)^2$, and M^2 can be the mass of K_{1A} or K_{1B}. Note that the matrix element we actually need in Eq. (11) requires $p_1 = p_2$. Thus, the F_2, F_3 terms in Eq. (12) vanish and only $F_1(q^2 = 0)$ is relevant. Accordingly, the mixing angle can be obtained as

$$\sin 2\theta_{K_1} = \frac{m_s - m_u}{m_{1400}^2 - m_{1270}^2}F_1(0). \tag{13}$$

III. HADRON LEVEL CALCULATION

In this section and the next, we will introduce a QCDSR calculation for the matrix element in Eq. (12). We first define a three-point correlation function,

$$\Pi_{\mu\nu\rho}(p_1, p_2) = i^2\int d^4x d^4y e^{ip_2\cdot x}e^{-ip_1\cdot y} \times \langle 0|T\{J_{\mu\nu}^{1B}(x)\bar{s}s(0)J_\rho^{1A\dagger}(y)\}|0\rangle, \tag{14}$$

where $J_{\mu\nu}^{1A}$ and $J_{\mu\nu}^{1B}$ are the currents of $K_{1A}(^3P_1)$ and $K_{1B}(^1P_1)$, respectively,

$$J_{\mu\nu}^{1B} = \bar{q}\sigma_{\mu\nu}s, \qquad J_\rho^{1A} = \bar{q}\gamma_\rho\gamma_5 s. \tag{15}$$

The correlation function defined in Eq. (14) should be calculated both at the hadron level and the quark-gluon level. At the hadron level, inserting the complete sets with the same quantum number of K_{1B} and K_{1A} into the correlation function and using the following definition of kaon decay constants:

$$\begin{aligned}\langle 0|J_{\mu\nu}^{1B}(0)|K_{1B}(p,\lambda)\rangle &= if_{K_{1B}}^\perp\epsilon_{\mu\nu\alpha\beta}\epsilon^\alpha(p,\lambda)p^\beta,\\ \langle 0|J_\rho^{1A}(0)|K_{1A}(p,\lambda)\rangle &= -if_{K_{1A}}m_{1A}\epsilon_\rho(p,\lambda),\\ \langle 0|J_\rho^{1A}(0)|K(p)\rangle &= if_K p_\rho,\end{aligned} \tag{16}$$

one can express the correlation function as

$$\begin{aligned}\Pi_{\mu\nu\rho}^H(p_1,p_2) = &-m_A f_A f_B^\perp\epsilon_{\mu\nu\alpha\beta}p_2^\beta\left(-g^{\alpha\kappa} + \frac{p_2^\alpha p_2^\kappa}{m_B^2}\right)\frac{1}{p_2^2 - m_{1B}^2}\left[F_1 g_{\kappa\tau} + \frac{F_2}{M^2}\epsilon_{\kappa\tau\rho\sigma}p_1^\rho p_2^\sigma + \frac{F_3}{M^2}p_{1\kappa}p_{2\tau}\right]\\ &\times\left(-g_\rho^\tau + \frac{p_1^\tau p_{1\rho}}{m_{1A}^2}\right)\frac{1}{p_1^2 - m_{1A}^2} + f_K f_{1B}^\perp\epsilon_{\mu\nu\alpha\beta}p_2^\beta p_{1\rho}\frac{1}{p_2^2 - m_{1B}^2}\left(-g^{\alpha\kappa} + \frac{p_2^\alpha p_2^\kappa}{m_{1B}^2}\right)p_{1\kappa}\frac{G(q^2)}{m_K}\frac{1}{p_1^2 - m_K^2}\\ &+\int_{s_1^{\rm th}}^\infty ds_1\int_{s_2^{\rm th}}^\infty ds_2\frac{\rho_{\mu\nu\rho}^{\rm conti}(s_1,s_2,q^2)}{(s_1 - p_1^2)(s_2 - p_2^2)} + \int_{s_1^{\rm th}}^\infty ds_1\frac{\rho_{1,\mu\nu\rho}^{\rm conti}(s_1,p_2,q^2)}{s_1 - p_1^2} + \int_{s_2^{\rm th}}^\infty ds_2\frac{\rho_{2,\mu\nu\rho}^{\rm conti}(p_1,s_2,q^2)}{s_2 - p_2^2}.\end{aligned} \tag{17}$$

The last three terms above denote the contribution from the excited and continuous spectrum, which begin at the thresholds $s_1^{\rm th}$ and $s_2^{\rm th}$. It should be noted that the axial-vector current J_ρ^{1A} can create both an axial vector and a pseudoscalar kaon from the vacuum. Therefore, to obtain Eq. (17), both the K_{1A} and K have been inserted between $\bar{s}s(0)$ and $J_\rho^{1A}(y)$, and we have used the parametrization for the $K \to K_{1B}$ matrix element,

$$\langle K_{1B}(p_2)|\bar{s}s(0)|K(p_1)\rangle = \epsilon_\mu^*(p_2)p_1^\mu\frac{G(q^2)}{m_K}, \tag{18}$$

where $G(q^2)$ is the corresponding form factor.

Now the hadron level correlation function in Eq. (17) depends on four form factors: F_1, F_2, F_3, G. However, only F_1 is relevant to the mixing angle as shown in Eq. (13). To remove the irrelevant form factors, we operate the following projection on the correlation function:

$$\epsilon^{\mu\rho\alpha\beta}p_1^\nu\Pi_{\mu\nu\rho}(p_1,p_2) = \tilde{\Pi}(p_1,p_2)(p_1^\beta p_2^\alpha - p_1^\alpha p_2^\beta). \tag{19}$$

$\tilde{\Pi}(p_1,p_2)$ is a newly defined scalar correlation function, which at hadron level only depends on F_1,

$$\tilde{\Pi}^H(p_1,p_2) = \frac{2m_{1A}f_{1A}f_{1B}^\perp F_1(q^2)}{(p_1^2 - m_{1A}^2)(p_2^2 - m_{1B}^2)} + \cdots, \tag{20}$$

where the ellipse denotes the last three terms in Eq. (17) with the projection defined in Eq. (19) being operated. In principle, the $\tilde{\Pi}(p_1,p_2)$ calculated at the hadron level and the quark-gluon level should be equivalent,

$$\tilde{\Pi}^H(p_1,p_2,q^2) = \tilde{\Pi}^{\rm QCD}(p_1,p_2,q^2) = \frac{1}{\pi^2}\int_{s_1^{\rm min}}^\infty ds_1\int_{s_2^{\rm min}}^\infty ds_2\frac{{\rm Im}^2\tilde{\Pi}^{\rm QCD}(s_1,s_2,q^2)}{(s_1 - p_1^2)(s_2 - p_2^2)}, \tag{21}$$

where $s_1^{\rm min} = s_2^{\rm min} = (m_s + m_q)^2$, where $q = u$ or d are the quark level thresholds. In the second equation above, we have expressed the $\tilde{\Pi}^{\rm QCD}$ as its dispersive integration form, with $s_1^{\rm min}$ and $s_2^{\rm min}$ being the quark level thresholds. According to the quark-hadron duality, the continuous spectrum contribution at hadron level is equivalent to that at QCD level. In other words, the ellipse term in Eq. (20) is equal to

$$\frac{1}{\pi^2}\left[\int_{s_1^{\mathrm{th}}}^{\infty} ds_1 \int_{s_2^{\mathrm{th}}}^{\infty} ds_2 + \int_{s_1^{\mathrm{th}}}^{\infty} ds_1 \int_{s_2^{\min}}^{s_2^{\mathrm{th}}} ds_2 + \int_{s_1^{\min}}^{s_1^{\mathrm{th}}} ds_1 \int_{s_2^{\mathrm{th}}}^{\infty} ds_2\right] \frac{\mathrm{Im}^2\tilde{\Pi}^{\mathrm{QCD}}(s_1,s_2,q^2)}{(s_1-p_1^2)(s_2-p_2^2)}. \quad (22)$$

Thus, the continuous spectrum contribution can be canceled at both the hadron and QCD levels. After Borel transformation, we arrive at the sum rules equation,

$$\mathcal{B}_{T_1,T_2}\{\tilde{\Pi}^H\}(q^2) = \mathcal{B}_{T_1,T_2}\{\tilde{\Pi}^{\mathrm{QCD}}\}(q^2),$$
$$2m_{1A}f_{1A}f_{1B}^{\perp}e^{-\frac{m_{1A}^2}{T_1^2}}e^{-\frac{m_{1B}^2}{T_2^2}}F_1(q^2) = \frac{1}{\pi^2}\int_{s_1^{\min}}^{s_1^{\mathrm{th}}} ds_1 \int_{s_2^{\min}}^{s_2^{\mathrm{th}}} ds_2\, e^{-\frac{s_1}{T_1^2}}e^{-\frac{s_2}{T_2^2}}\mathrm{Im}^2\tilde{\Pi}^{\mathrm{QCD}}(s_1,s_2,q^2), \quad (23)$$

where T_1, T_2 are the two Borel parameters corresponding to p_1^2, p_2^2. Now it is clear that F_1 can be obtained through Eq. (23) if the imaginary part of $\tilde{\Pi}^{\mathrm{QCD}}$ is calculated.

IV. QUARK-GLUON LEVEL CALCULATION

A. Perturbative diagram

In this section, we present the QCD level calculation for $\tilde{\Pi}^{\mathrm{QCD}}$ and extract its imaginary part. In the deep Euclidean region $p_1^2, p_2^2, q^2 \ll 0$, $\tilde{\Pi}^{\mathrm{QCD}}$ can be analytically calculated by operator product expansion (OPE).

The leading contribution to OPE is from the perturbation diagram as shown by the left diagram in Fig. 1, with amplitude

$$\Pi^{\mathrm{pert}}_{\mu\nu\rho}(p_1,p_2,q^2) = \frac{iN_c}{(2\pi)^4}\int d^4k_1 d^4k_2 d^4k\,\delta^4(p_2-k_2-k)\delta^4(p_1-k_1-k) \times \frac{\mathrm{tr}[\not{k}\sigma_{\mu\nu}(\not{k}_2+m_s)(\not{k}_1+m_s)\gamma_\rho\gamma_5]}{k^2(k_2^2-m_s^2)(k_1^2-m_s^2)}. \quad (24)$$

The double imaginary part of the correlation function is related with its double discontinuity as

$$\mathrm{Im}^2\Pi^{\mathrm{pert}}_{\mu\nu\rho}(p_1,p_2,q^2) = \frac{1}{(2i)^2}\mathrm{Disc}^2\Pi^{\mathrm{pert}}_{\mu\nu\rho}(p_1,p_2,q^2)$$
$$= \frac{1}{(2i)^2}\frac{iN_c}{(2\pi)^4}(-2\pi i)^3\int d\Phi_\Delta(p_1,p_2,m_s,m_s,0) \times \mathrm{tr}[\not{k}\sigma_{\mu\nu}(\not{k}_2+m_s)(\not{k}_1+m_s)\gamma_\rho\gamma_5], \quad (25)$$

which is obtained by the cutting rules: $\mathrm{Disc}\{1/(p^2-m^2+i\epsilon)\} = (-2\pi i)\delta(p^2-m^2)$. In the above expression, we have introduced a three-body phase space integration measure $d\Phi_\Delta$ for a triangle integration as shown by the right diagram in Fig. 1,

$$\int d\Phi_\Delta(p_1,p_2,m_1,m_2,m) = \int d^4k_1 d^4k_2 d^4k\,\delta(k_1^2-m_1^2)\delta(k_2^2-m_2^2)\delta(k^2-m^2) \times \delta^4(p_2-k_2-k)\delta^4(p_1-k_1-k), \quad (26)$$

where the three internal lines are set on shell. The scalar triangle integration with unit integrand reads as

$$I_\Delta = \int d\Phi_\Delta(p_1,p_2,m_1,m_2,m)\cdot 1 = \frac{\pi}{2\sqrt{\lambda}} \times \Theta[s_1,s_2,q^2,m_1,m_2,m]\theta[s_1-s_1^{\min}]\theta[s_2-s_2^{\min}], \quad (27)$$

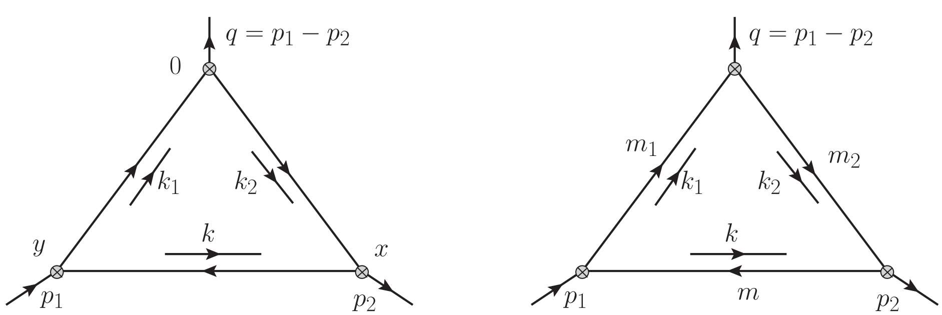

FIG. 1. The perturbative diagram contribution to the correlation function, where the lower two vertices denote the kaon currents defined in Eq. (15) (left). A general triangle diagram corresponding to a three-point correlation function (right).

where $\lambda=(s_1+s_2-q^2)^2-4s_1s_2$ with $p_1^2=s_1$, $p_2^2=s_2$. Θ is a θ function constraining the s_1, s_2, q^2,

$$\begin{aligned}&\Theta[s_1,s_2,q^2,m_1,m_2,m]\\&=\theta[-m_2^4s_1-m_1^4s_2+m_2^2[m^2(q^2+s_1-s_2)\\&\quad+s_1(q^2-s_1+s_2)]\\&\quad-q^2(m^4+s_1s_2-m^2(-q^2+s_1+s_2))\\&\quad+m_1^2[(q^2+s_1-s_2)s_2\\&\quad+m^2(q^2-s_1+s_2)+m_2^2(-q^2+s_1+s_2)]]. \qquad (28)\end{aligned}$$

The rest of the two θ functions ensure that s_1, s_2 are above the corresponding quark level thresholds, namely, $s_{1,2}>s_{1,2}^{\min}=(m_{1,2}+m)^2$. In Eq. (25), one has to set $m_1=m_2=m_s$. The definitions and expressions of higher rank triangle diagram integrations are given in Appendix A. The analytical expression of $\mathrm{Im}^2\tilde{\Pi}^{\mathrm{pert}}(p_1,p_2,q^2)$ is given in Appendix B.

B. $\bar{q}q$ condensate diagrams

The dimension-three operator contribution to OPE comes from the quark condensing diagrams as shown in Fig. 2. It can be found that the amplitudes of the s quark condensing diagrams are only proportional to $1/(p_1^2-m_s^2)$ or $1/(p_2^2-m_s^2)$, but not $1/(p_1^2-m_s^2)(p_2^2-m_s^2)$. Therefore, Figs. 2(b) and 2(c) will vanish under the double Borel transformation which operates on p_1^2 and p_2^2 simultaneously. The amplitude of Fig. 2(a) reads as

$$\begin{aligned}\Pi^{\bar{q}q}_{\mu\nu\rho}(p_1,p_2,q^2)&=i^2\int d^4xd^4y\,e^{ip_2\cdot x}e^{-ip_1\cdot y}\\&\quad\times[\sigma_{\mu\nu}D_s^{(0)}(x,0)D_s^{(0)}(0,y)\gamma_\rho\gamma_5]\\&\quad\times\langle 0|\bar{q}_a^i(x)q_b^i(y)|0\rangle, \qquad (29)\end{aligned}$$

where $D_s^{(0)}$ denotes the free s quark propagator. The nonlocal $\bar{q}q$ condensing matrix element can be expanded up to dimension-five local operators as [41]

$$\begin{aligned}&\langle 0|\bar{q}_a^i(x)q_b^i(y)|0\rangle\\&=N_c\left[\langle\bar{q}q\rangle\frac{1}{12}\delta_{ba}+\langle\bar{q}Gq\rangle\frac{1}{192}(x-y)^2\delta_{ba}\right]. \qquad (30)\end{aligned}$$

The contribution of the dimension-three operator, namely, the $\bar{q}q$ condensate, only comes from the first term given above. The Borel transformed $\tilde{\Pi}^{\bar{q}q}$ reads as

$$\mathcal{B}_{T_1,T_2}\{\tilde{\Pi}^{\bar{q}q}\}(p_1,p_2,q^2)=\frac{2}{3}N_cm_s\langle\bar{q}q\rangle e^{-m_s^2/T_1^2-m_s^2/T_2^2}. \qquad (31)$$

The second term in Eq. (30) provides a contribution from the dimension-five operator $\bar{q}g_sG_{\alpha\beta}q$. The corresponding amplitude reads as

$$\begin{aligned}&\Pi^{\bar{q}Gq(1)}_{\mu\nu\rho}(p_1,p_2,q^2)\\&=\frac{N_c}{192}\langle\bar{q}Gq\rangle(-1)\left(\frac{\partial^2}{\partial p_2^\alpha\partial p_{2\alpha}}+\frac{\partial^2}{\partial p_1^\alpha\partial p_{1\alpha}}+2\frac{\partial^2}{\partial p_1^\alpha\partial p_{2\alpha}}\right)\\&\quad\times\mathrm{tr}[\sigma_{\mu\nu}(\not{p}_2+m_s)(\not{p}_1+m_s)\gamma_\rho\gamma_5]\\&\quad\times\frac{1}{p_1^2-m_s^2}\frac{1}{p_2^2-m_s^2}, \qquad (32)\end{aligned}$$

where we have transformed x, y to $-i\partial/\partial p_2, i\partial/\partial p_1$ through the exponential terms in Eq. (29). To simplify the calculation of Eq. (32), we can omit the terms suppressed by m_s^2 and obtain

$$\begin{aligned}&\Pi^{\bar{q}Gq(1)}_{\mu\nu\rho}(p_1,p_2,q^2)\\&=-\frac{N_c}{12}\langle\bar{q}Gq\rangle m_s\epsilon_{\mu\nu\rho\alpha}(p_1^\alpha-p_2^\alpha)\frac{\partial}{\partial M^2}\\&\quad\times\left[\frac{1}{(p_1^2-M^2)(p_2^2-m_s^2)}-\frac{1}{(p_1^2-m_s^2)(p_2^2-M^2)}\right]\Bigg|_{M^2=m_s^2}\\&\quad-\frac{N_c}{12}\langle\bar{q}Gq\rangle m_s\epsilon_{\mu\nu\rho\alpha}(p_1^\alpha+p_2^\alpha)q^2\\&\quad\times\frac{\partial^2}{\partial M_1^2\partial M_2^2}\left[\frac{1}{(p_1^2-M_1^2)(p_2^2-M_2^2)}\right]\Bigg|_{M_1^2=M_2^2=m_s^2}. \qquad (33)\end{aligned}$$

To obtain the above expression, we have introduced derivatives on auxiliary masses M_1, M_2 to lower the power of the denominator, which means

$$\frac{1}{(p_{1,2}^2-m_{1,2}^2)^2}=\frac{\partial}{\partial M^2}\frac{1}{p_{1,2}^2-M^2}\Bigg|_{M^2\to m_{1,2}^2}. \qquad (34)$$

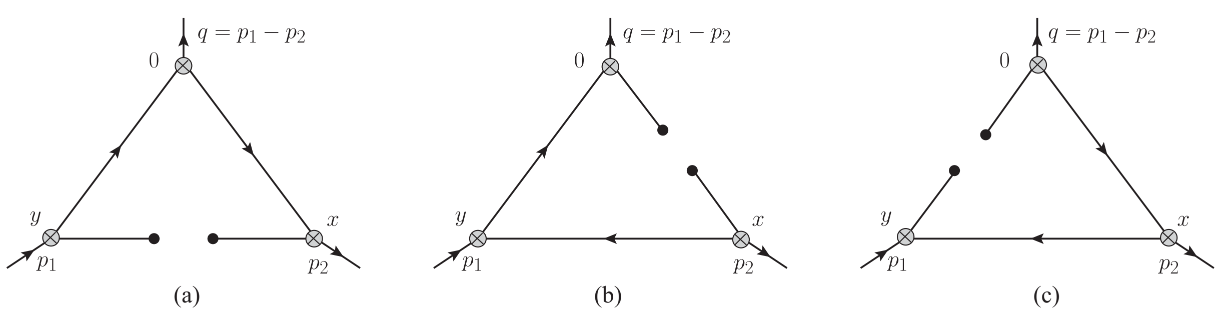

FIG. 2. The $\bar{q}q$ condensate diagram contribution to the correlation function, where one of the quark lines is disconnected. The diagrams in (b) and (c) will vanish under the double Borel transformation for p_1^2 and p_2^2 simultaneously. Diagram (a) is the only nonvanishing diagram.

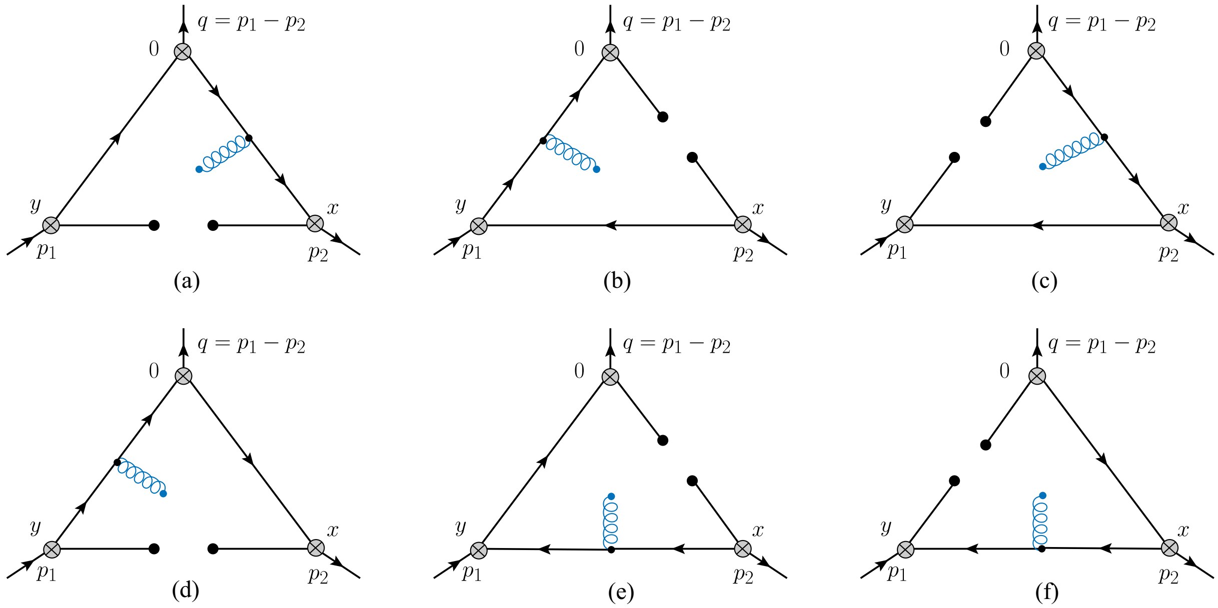

FIG. 3. The $\bar{q}Gq$ condensate diagram contribution to the correlation function, where one of the quark lines emits a soft gluon, which condenses with the other two disconnected quark fields. (b), (c), (e), (f) Diagrams vanish under double Borel transformation. (d) Diagram vanishes under the projection introduced in Eq. (19). Diagram (a) is the only nonvanishing diagram.

Taking the imaginary part, using dispersive integration, and conducting Borel transformation, we arrive at

$$\mathcal{B}_{T_1,T_2}\{\tilde{\Pi}^{\bar{q}Gq(1)}\}(q^2) = \frac{1}{6}N_c m_s\langle\bar{q}Gq\rangle \times e^{-m_s^2/T_1^2 - m_s^2/T_2^2}\left[\frac{1}{T_1^2} - \frac{1}{T_2^2} + \frac{q^2}{T_1^2 T_2^2}\right]. \tag{35}$$

C. $\bar{q}Gq$ condensate diagrams

The quark-gluon condensing diagrams are shown in Fig. 3, where a quark interacts with a background gluon field that condensates with the other two disconnected light quark fields. These diagrams provide the dimension-five operator contribution in the OPE. The massive and massless quark propagators in the background gluon field read as [41]

$$D_s(x,0) = i\int\frac{d^4k}{(2\pi)^4}e^{-ik\cdot x}\left[\frac{\delta_{ij}}{\not{k} - m_s} - \frac{g_s G^A_{\alpha\beta}t^A_{ij}}{4}\frac{\sigma^{\alpha\beta}(\not{k}+m_s) + (\not{k}+m_s)\sigma^{\alpha\beta}}{(k^2-m_s^2)^2} - \frac{g_s^2(t^At^B)_{ij}G^A_{\alpha\beta}G^B_{\mu\nu}[f^{\alpha\beta\mu\nu}(k) + f^{\alpha\mu\beta\nu}(k) + f^{\alpha\mu\nu\beta}(k)]}{4(k^2-m_s^2)^2} + \cdots\right],$$
$$D_q(x,0) = \frac{i\delta_{ij}\not{x}}{2\pi^2x^4} - \frac{ig_sG^A_{\alpha\beta}t^A_{ij}(\not{x}\sigma^{\alpha\beta} + \sigma^{\alpha\beta}\not{x})}{32\pi^2x^2} + \cdots, \tag{36}$$

where

$$f^{\alpha\beta\mu\nu}(k) = (\not{k}+m_s)\gamma^\alpha(\not{k}+m_s)\gamma^\beta(\not{k}+m_s)\gamma^\mu(\not{k}+m_s)\gamma^\nu(\not{k}+m_s), \tag{37}$$

and we have only present the terms relevant to the OPE up to dimension-five operators in Eq. (36).

It can be found that the diagrams in Figs. 3(b), 3(c), 3(e), and 3(f) in vanish after the Borel transformation due to the same reason as what happens in the $\bar{q}q$ condensate diagrams. The Fig. 3(d) vanishes after the projection introduced in Eq. (19). Thus, Fig. 3(a) is the only nonvanishing diagram with amplitude

$$\Pi^{\bar{q}Gq(2)}_{\mu\nu\rho}(p_1,p_2,q^2) = i^2\int d^4xd^4ye^{ip_2\cdot x}e^{-ip_1\cdot y}\int\frac{d^4k_1}{(2\pi)^4}\frac{d^4k_2}{(2\pi)^4}e^{ik_1\cdot y}e^{-ik_2\cdot x} \times\left[\sigma_{\mu\nu}\left(\frac{-i}{4}\right)\frac{\sigma^{\alpha\beta}(\not{k}_2+m_s) + (\not{k}_2+m_s)\sigma^{\alpha\beta}}{(k_2^2-m_s^2)^2}\frac{i(\not{k}_1+m_s)}{k_1^2-m_s^2}\gamma_\rho\gamma_5\right]_{ab}t^A_{ij}\langle 0|\bar{q}^i_a(x)g_sG^A_{\alpha\beta}(0)q^i_b(y)|0\rangle. \tag{38}$$

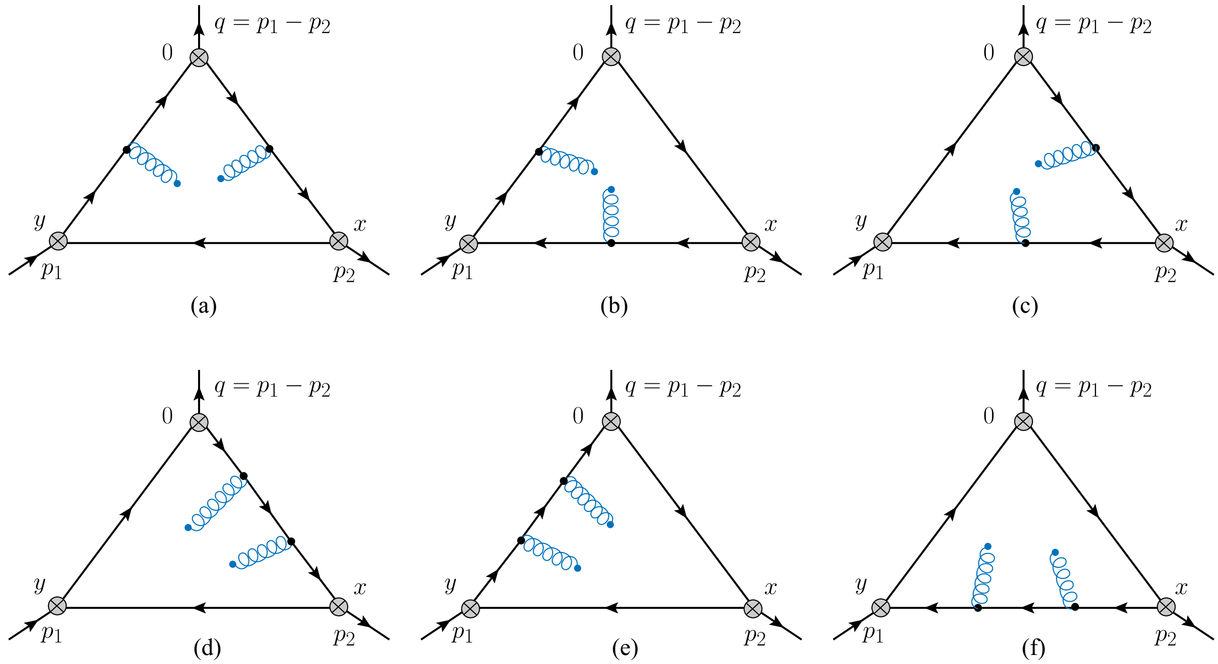

FIG. 4. The GG condensate diagram contribution to the correlation function, where two soft gluons are emitted from the internal quark lines and condensate with each other. (d)–(f) Diagrams can be neglected in this calculation since (d),(e) are suppressed by m_s^2, while (f) is suppressed by m^2. Only the diagrams (a), (b), (c) contribute.

Using the quark-gluon condensate formula, keeping the leading term

$$\langle 0|\bar{q}_a^i(x) g_s G_{\alpha\beta}^A(0) q_b^i(y)|0\rangle = \frac{1}{192}\langle \bar{q}Gq\rangle (\sigma_{\alpha\beta})_{ba} t_{ji}^A + \cdots, \tag{39}$$

and conducting the projection introduced in Eq. (19), we can obtain

$$\begin{aligned}&\tilde{\Pi}^{\bar{q}Gq(2)}(p_1, p_2, q^2)\\ &\quad = \frac{1}{24} m_s \langle \bar{q}Gq\rangle \frac{\partial}{\partial M^2} \frac{1}{(p_1^2 - m_s^2)(p_2^2 - M^2)}\bigg|_{M^2 = m_s^2}.\end{aligned} \tag{40}$$

The Borel transformed form reads as

$$\mathcal{B}_{T_1,T_2}\{\tilde{\Pi}^{\bar{q}Gq(2)}\}(q^2) = -\frac{1}{6} m_s \langle \bar{q}Gq\rangle \frac{1}{T_2^2} e^{-m_s^2/T_1^2} e^{-m_s^2/T_2^2}. \tag{41}$$

D. GG condensate diagrams

The gluon-gluon condensate diagrams are shown in Fig. 4, where the internal quarks interact with two soft background gluon fields that condensate in the vacuum. These diagrams provide the dimension-four operator contribution in the OPE. In Fig. 4(a), both the two s quarks interact with the background gluons, and the corresponding amplitude reads as

$$\begin{aligned}\Pi_{\mu\nu\rho}^{GG(a)}(p_1, p_2, q^2) = {}& \int d^4x d^4y\, e^{ip_2\cdot x} e^{-ip_1\cdot y} \int \frac{d^4k_1}{(2\pi)^4} \frac{d^4k_2}{(2\pi)^4} \frac{d^4k}{(2\pi)^4} e^{ik_1\cdot y} e^{-ik_2\cdot x} e^{-ik\cdot(y-x)} \left(-\frac{i}{4}\right)^2\\ &\times \mathrm{tr}\left[\frac{-i\not{k}}{k^2}\sigma_{\mu\nu} \frac{\sigma^{\alpha\beta}(\not{k}_2 + m_s) + (\not{k}_2 + m_s)\sigma^{\alpha\beta}}{(k_2^2 - m_s^2)^2} \frac{\sigma^{\kappa\tau}(\not{k}_1 + m_s) + (\not{k}_1 + m_s)\sigma^{\kappa\tau}}{(k_2^2 - m_s^2)^2}\gamma_\rho\gamma_5\right]\\ &\times \mathrm{tr}[t^A t^B] g_s^2 \langle 0|G_{\alpha\beta}^A(0) G_{\kappa\tau}^B(0)|0\rangle.\end{aligned} \tag{42}$$

Using the gluon condensate formula

$$g_s^2\langle 0|G_{\alpha\beta}^A(0) G_{\kappa\tau}^B(0)|0\rangle = \frac{1}{96}\langle GG\rangle \delta_{AB}(g_{\alpha\kappa}g_{\beta\tau} - g_{\alpha\tau}\beta\kappa), \tag{43}$$

and extracting the imaginary part by cutting rules, we arrive at

$$\begin{aligned}\mathrm{Im}^2\Pi^{GG(a)}_{\mu\nu\rho}(p_1,p_2,q^2) = {} & \frac{1}{3072\pi}\frac{\partial^2}{\partial M_1^2\partial M_2^2}\int d\Phi_\Delta[p_1,p_2,M_1,M_2,0] \\ & \times \mathrm{tr}[\not{k}\sigma_{\mu\nu}(\sigma^{\alpha\beta}(\not{k}_2+m_s)+(\not{k}_2+m_s)\sigma^{\alpha\beta}) \\ & \times (\sigma^{\kappa\tau}(\not{k}_1+m_s)+(\not{k}_1+m_s)\sigma^{\kappa\tau})\gamma_\rho\gamma_5] \end{aligned} \tag{44}$$

$$\times\,(g_{\alpha\kappa}g_{\beta\tau}-g_{\alpha\tau}\beta\kappa)|_{M_1^2=m_s^2,M_2^2=m_s^2}. \tag{45}$$

Note that before doing the derivative on the auxiliary masses we must temporary change the invariant mass square of the k_1, k_2 lines to be M_1^2, M_2^2. The analytical result of $\mathrm{Im}^2\tilde{\Pi}^{GG(k_1k_2)}$ is given in Appendix B.

In Figs. 4(b) and 4(c), one of the two condensing gluons comes from the massless quark. The massless quark propagator in the background gluon field has been given by Eq. (36) with the use of coordinate space. The amplitude of Fig. 4(b) reads as

$$\begin{aligned}\Pi^{GG(b)}_{\mu\nu\rho}(p_1,p_2,q^2) = {} & \int d^4x d^4y\, e^{ip_2\cdot x}e^{-ip_1\cdot y}\int\frac{d^4k_1}{(2\pi)^4}\frac{d^4k_2}{(2\pi)^4}e^{ik_1\cdot y}e^{-ik_2\cdot x}\left(-\frac{i}{32\pi^2}\right)\left(-\frac{i}{4}\right)\mathrm{tr}[t^At^B] \\ & \times\mathrm{tr}\left[\frac{(\not{y}-\not{x})\sigma^{\kappa\tau}+\sigma^{\kappa\tau}(\not{y}-\not{x})}{(y-x)^2}\sigma_{\mu\nu}\frac{i(\not{k}_2+m_s)}{k_2^2-m_s^2}\frac{\sigma^{\alpha\beta}(\not{k}_1+m_s)+(\not{k}_1+m_s)\sigma^{\alpha\beta}}{(k_1^2-m_s^2)^2}\gamma_\rho\gamma_5\right] \\ & \times g_s^2\langle 0|G^A_{\alpha\beta}(0)G^B_{\kappa\tau}(0)|0\rangle. \end{aligned} \tag{46}$$

Redefining the coordinate: $w=y-x$ and using the integration formula in the coordinate space,

$$\int d^4w\, e^{-i(p_1-k_1)\cdot w}\frac{1}{w^2}=(-4\pi^2 i)\frac{1}{(p_1-k_1)^2}, \tag{47}$$

we have the imaginary part as

$$\begin{aligned} & \mathrm{Im}^2\tilde{\Pi}^{GG(b)}(p_1,p_2,q^2)(p_1^{\beta'}p_2^{\alpha'}-p_2^{\alpha'}p_2^{\beta'}) \\ & = -\frac{1}{6144\pi}\langle GG\rangle\epsilon^{\mu\rho\alpha'\beta'}p_1^\nu\frac{\partial}{\partial M_1^2}\left(\frac{\partial}{\partial p_1^\sigma}+\frac{\partial}{\partial p_2^\sigma}\right) \\ & \quad\times\int d\Phi_\Delta[p_1,p_2,M_1,m_s,0][g_{\alpha\kappa}g_{\beta\tau}-g_{\alpha\tau}g_{\beta\kappa}] \\ & \quad\times\mathrm{tr}[(\gamma^\sigma\sigma^{\kappa\tau}+\sigma^{\kappa\tau}\gamma^\sigma)\sigma_{\mu\nu}(\sigma^{\alpha\beta}(\not{k}_2+m_s) \\ & \quad+(\not{k}_2+m_s)\sigma^{\alpha\beta})(k_1^2-m_s^2)\gamma_\rho\gamma_5]|_{M_1^2=m_s^2}, \end{aligned} \tag{48}$$

where the linear term of w has been transformed to the derivatives of p_1, p_2. The calculation of Fig. 4(c) is almost the same, so it will not be presented here.

It can be found that the amplitude of Fig. 4(f) is proportional to m^2, which vanishes by ignoring the u, d masses. On the other hand, the amplitudes of Figs. 4(d) and 4(e) are proportional to m_s^2. Compared with Figs. 4(a)–4(c), they only produce $\mathcal{O}(m_s^2)$ suppressed contributions to $F_1(0)$ and thus can be neglected. On the other hand, in Eq. (13) the expression of $\sin 2\theta_{K_1}$ has already been proportional to m_s^2. Thus, ignoring the terms proportional to m_s^2 in $F_1(0)$ is reasonable since they only produce $\mathcal{O}(m_s^3)$ corrections to $\sin 2\theta_{K_1}$. Therefore, Figs. 4(d) and 4(e) will not be considered in this work. In Appendix B, we present the analytical results of Figs. 4(a)–4(c), and take Fig. 4(e) as an example to show how Figs. 4(d)–4(f) are suppressed by the quark mass square.

V. NUMERICAL RESULTS

The masses of K_{1A}, K_{1B} and their decay constants are taken from Ref. [42]: $m_{1A}=1.31\pm0.06$, $m_{1B}=1.34\pm0.08$, $f_{1A}=0.25\pm0.013$, and $f_{1B}=0.19\pm0.01$ GeV. In this work, we set $m_u=m_d=0$, and $m_s=(0.1\pm0.005)$ GeV at the energy scale $\mu\sim m_{1A,1B}=1.3$ GeV [43]. The condensate parameters are taken as [44,45] $\langle\bar{q}q\rangle=-(0.24\pm0.01\text{ GeV})^3$, $\langle\bar{q}Gq\rangle=m_0^2\langle\bar{q}q\rangle$ with $m_0^2=(0.8\pm0.2)\text{ GeV}^2$, and $\langle GG\rangle=(4\pi^2)(0.012\pm0.004)\text{ GeV}^4$.

In terms of the threshold parameters, note that, since J^{1A}_ρ can create both pseudoscalar and axial-vector kaons, the next excited states should begin from the pseudoscalar $K(1460)$. On the other hand, $J^{1B}_{\mu\nu}$ can only create axial-vector kaons, thus the next excited states begin from the axial vector $K_1(1650)$. Generally, in QCDSRs the threshold parameter is chosen slightly below the next excited state; therefore, one has to set s_1^{th} and s_2^{th} in a region nearly below $m^2_{K(1460)}$ and $m^2_{K(1650)}$, respectively. For simplicity, we can correlate s_1^{th} and s_2^{th} and parametrize them by the same parameter τ_{th},

$$\begin{aligned} s_1^{\mathrm{th}} &= m_{1A}^2+\tau_{\mathrm{th}}(m^2_{K(1460)}-m_{1A}^2), \\ s_2^{\mathrm{th}} &= m_{1B}^2+\tau_{\mathrm{th}}(m^2_{K(1650)}-m_{1B}^2), \end{aligned} \tag{49}$$

so that s_1^{th} and s_2^{th} increase or decrease simultaneously when varying τ_{th} in the region $0<\tau_{\mathrm{th}}<1.0$, and both reach the next excited states $m^2_{K(1460)}$ and $m^2_{K(1650)}$ at $\tau_{\mathrm{th}}=1.0$. The region closely below the excited states corresponds to

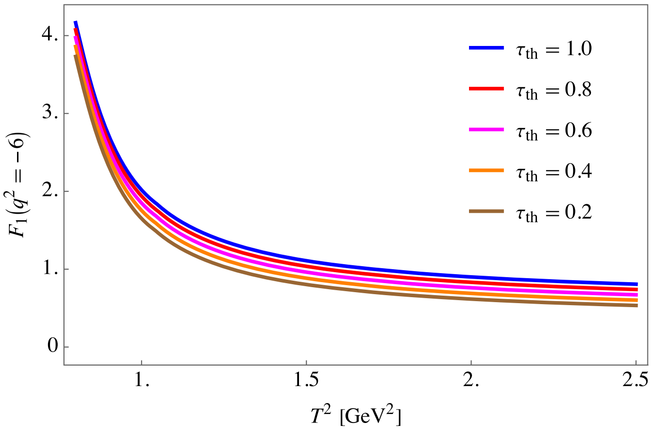

FIG. 5. F_1 as a function of T^2 at $q^2 = -6$ GeV with different choices of $s^{\rm th}_{1,2}$.

$\tau_{\rm th} \lesssim 1.0$, which will be chosen as $0.6 < \tau_{\rm th} < 1.0$ for the following error analysis.

Then one has to check the behavior of F_1 as a function of the Borel parameters when varying $s^{\rm th}_{1,2}$. Note that the mass difference between the initial and final kaon is little, and the Borel parameters are closely related with the corresponding hadron masses; thus, one can simply choose $T_1 = T_2 = T$. Without loss of generality, q^2 can be chosen by an arbitrary value in the deep Euclidean region when investigating the T^2 dependence. Here we choose $q^2 = -6$ GeV^2, and then the $F_1(-6)$ as functions of T^2 with different choices of $\tau_{\rm th}$ are shown in Fig. 5. It can be found that the variation of $F_1(T^2)$ is small when adjusting $\tau_{\rm th}$, especially at the region nearly below the excited states: $\tau_{\rm th} \lesssim 1$. On the other hand, all the curves in Fig. 5 turn to be stable when T^2 is large, especially at the region $T^2 > 1.5$ GeV^2. However, since there is no maximum or minimum point appearing in Fig. 5, one has to use further reasonable requirements to seek the feasible region of the Borel parameter.

The determination of Borel parameters depends on two criteria. First, the contribution from the continuous spectrum must be suppressed so that it is smaller than the pole contribution. Quantitatively, this criterion can be expressed by the constraint

$$\xi_{\rm conti} \equiv \frac{\int_{s_1^{\rm th}}^{\infty} ds_1 \int_{s_2^{\rm th}}^{\infty} ds_2\, e^{-\frac{s_1}{T_1^2}} e^{-\frac{s_2}{T_2^2}} {\rm Im}^2 \tilde{\Pi}^{\rm QCD}(s_1, s_2, q^2)}{\int_0^{\infty} ds_1 \int_0^{\infty} ds_2\, e^{-\frac{s_1}{T_1^2}} e^{-\frac{s_2}{T_2^2}} {\rm Im}^2 \tilde{\Pi}^{\rm QCD}(s_1, s_2, q^2)} \lesssim 0.5, \tag{50}$$

where the numerator denotes the contribution from the continuous spectrum, while the denominator denotes all the spectrum contributions. We still choose $q^2 = -6$ GeV^2 and present $\xi_{\rm conti}$ as a function of T^2 in the left diagram of Fig. 6, where the blue and red bands denote the errors from the uncertainties of condensate parameters and $m_{K_{1A}}, f_{1A}, f^{\perp}_{1B}$, respectively. The purple band shows the uncertainty of $\tau_{\rm th}$ in the region $0.6 < \tau_{\rm th} < 1.0$, which as shown by Eq. (49) describes the threshold parameters closely below the excited states: $m^2_{K(1460)}$ and $m^2_{K(1650)}$. It can be found that $\xi_{\rm conti}$ increases with the increasing of T^2. $\xi_{\rm conti} = 50\%$ occurs at $T^2 = 1.16$–2.39 GeV^2, which gives the range of the upper limit for the Borel parameter,

$$1.16 < T^2_{\rm upper} < 2.39\ {\rm GeV}^2. \tag{51}$$

The second criterion demands the convergence of OPE. First, we have to compare the perturbative contribution and all the condensate contributions. The right diagram of Fig. 6 shows the fraction of the condensate and the perturbative contribution,

$$\eta_{\rm cond} \equiv \frac{|F_1^{\bar{q}q} + F_1^{GG} + F_1^{\bar{q}Gq}|}{|F_1^{\rm pert}|}. \tag{52}$$

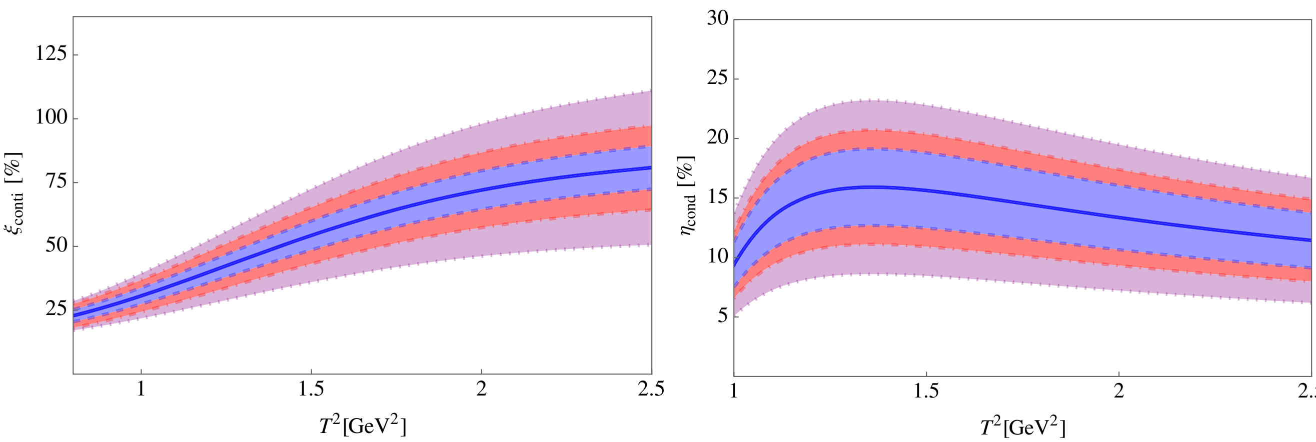

FIG. 6. $\xi_{\rm conti}$ as a function of T^2 (left) and $\eta_{\rm cond}$ as a function of T^2 (right), with $q^2 = -6$ GeV^2. The blue and red bands denote the errors from the uncertainties of condensate parameters and $m_{K_{1A}}, f_{1A}, f^{\perp}_{1B}$, respectively. The purple band comes from the uncertainty of $\tau_{\rm th}$ in the region $0.6 < \tau_{\rm th} < 1.0$.

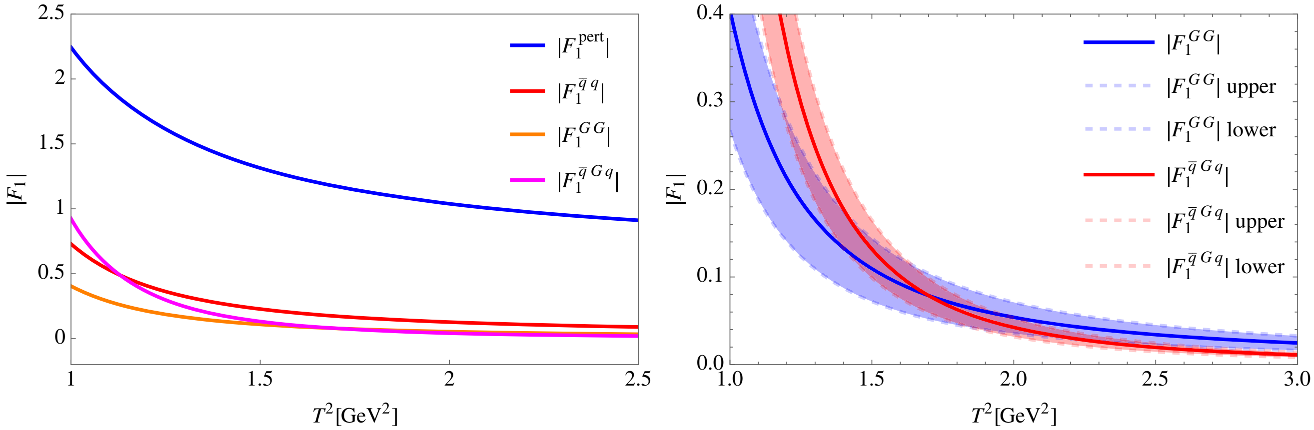

FIG. 7. Absolute F_1 contributed from various condensate diagrams at $q^2 = -6\ \mathrm{GeV}^2$ (left). A detailed comparison of the GG and $\bar{q}Gq$ condensate contributions to the absolute F_1 (right), where the error bands denote the combined uncertainties from the condensates $\langle GG\rangle$, $\langle \bar{q}Gq\rangle$, and the threshold $0.6 < \tau_{\rm th} < 1.0$.

It can be found that $\eta_{\rm cond} < 1$ is safely satisfied in a wide T^2 range. Next, we have to exam whether the F_1 contributed from a higher dimension condensate is smaller than that from a lower one. In other words, the following inequality equation should be checked:

$$|F_1^{\rm pert}| > |F_1^{\bar{q}q}| > |F_1^{GG}| > |F_1^{\bar{q}Gq}|. \tag{53}$$

The left diagram in Fig. 7 shows the absolute F_1 contributed from various condensate diagrams with $q^2 = -6\ \mathrm{GeV}^2$. It is obvious that the perturbative diagram contribution is larger than all the other condensate contributions. Furthermore, $|F_1^{\bar{q}q}|$ is also larger than $|F_1^{GG}|$ and $|F_1^{\bar{q}Gq}|$ in the large T^2 region. However, there seems to be an ambiguity when comparing $|F_1^{GG}|$ and $|F_1^{\bar{q}Gq}|$. Thus, a detailed comparison between them is presented by the right diagram in Fig. 7, where the error bands denote the combined uncertainties from the condensates $\langle GG\rangle$, $\langle \bar{q}Gq\rangle$, and the threshold $0.6 < \tau_{\rm th} < 1.0$. Demanding $|F_1^{GG}| > |F_1^{\bar{q}Gq}|$ and considering the uncertainty band, one can obtain the range of the lower limit for the Borel parameter,

$$1.17 < T^2_{\rm lower} < 2.64\ \mathrm{GeV}^2, \tag{54}$$

which intersects with the upper limit range given by Eq. (51). Therefore, combining Eqs. (51) and (54), one can obtain the window for T^2 as

$$1.17 < T^2 < 2.39\ \mathrm{GeV}^2. \tag{55}$$

According to Eq. (13), one can obtain θ_{K_1} as a function of T^2 directly by knowing the T^2 behavior of $F_1(0)$ and then determine the exact value of θ_{K_1} in the T^2 window: $1.17 \lesssim T^2 \lesssim 2.39\ \mathrm{GeV}^2$. However, instead of the physical region, with the QCDSR calculation, only the deep Euclidean region result $F_1(q^2 \ll 0)$ is known. Therefore, $F_1(q^2 \geq 0)$ should be obtained by analytic continuation from the deep Euclidean region. In this work, to realize the analytic continuation, a single pole formula

$$F_1(q^2) = \frac{F_1(0)}{1 - q^2/m^2_{\rm pole}} \tag{56}$$

is used to fit $F_1(q^2)$, where $F_1(0)$ and $m_{\rm pole}$ play the role of fitting parameters. The fitting region is chosen as $-10 < q^2 < -3\ \mathrm{GeV}^2$ so that the spectral integrals can be calculated safely by applying cutting rules. The $m_{\rm pole}$ as a function of T^2 is shown in the left diagram of Fig. 8. Before transforming $F_1(0)$ to θ_{K_1} by Eq. (13), it should be mentioned that $F_1(0)$ has sign ambiguity due to the sign ambiguity of the decay constants f_{1A} and $f_{1B}^\perp$ derived with QCDSRs in Ref. [42]. The reason is that, when using a two-point correlation in QCDSRs to calculate f_{1A} or $f_{1B}^\perp$, one can only determine their square and thus the exact sign cannot be determined. Considering the sign ambiguity, we present the absolute value of θ_{K_1} as a function of T^2 in the right diagram of Fig. 8. Including the effect of error bands, we obtain the mixing angle as $|\theta_{K_1}| = 21.4^\circ \pm 9^\circ$. Note that both θ_{K_1} and $90^\circ - \theta_{K_1}$ are the solutions to Eq. (13). Therefore, another possible mixing angle value is $|\theta'_{K_1}| = 68.6^\circ \pm 9^\circ$.

In Table I, we compare our result for $|\theta_{K_1}|$ with those obtained in the literature by various methods:

(1) using early experimental information on masses and the partial rates of $K_1(1270)$ and $K_1(1400)$ [22];
(2) phenomenologically analyzing the τ weak decays: $\tau \to K_1(1270)\nu_\tau$ and $\tau \to K_1(1400)\nu_\tau$ [23,24];
(3) analyzing the $f_1(1285) - f_1(1420)$ mixing angle $\theta_{^3P_1}$ and its correlation to θ_{K_1} [25];
(4) analyzing both the mixing angle of $f_1(1285) - f_1(1420)$ and $h_1(1170) - h_1(1380)$ [26];

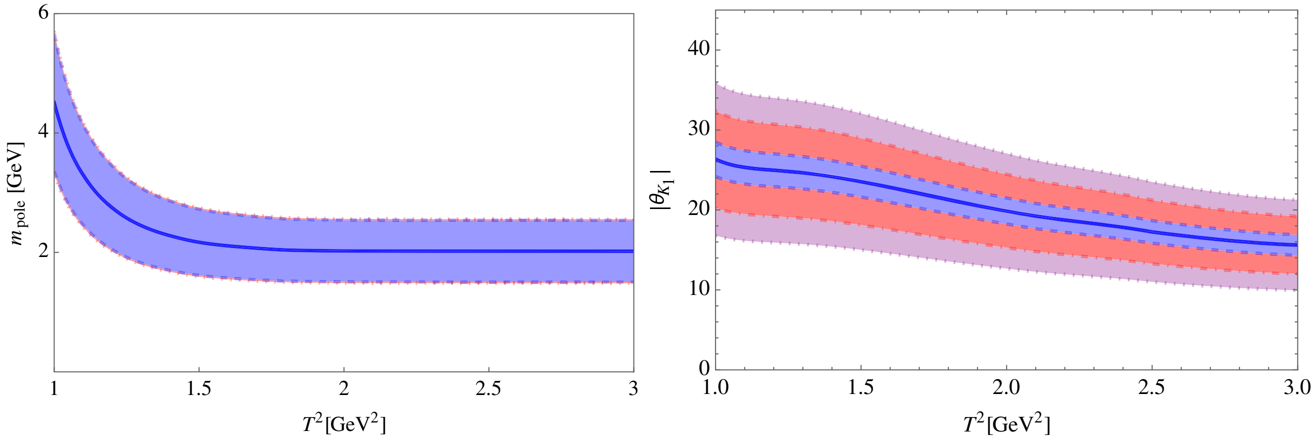

FIG. 8. m_{pole} as a function of T^2, where the blue band denotes the combined uncertainties of τ_{th} in the region $0.6 < \tau_{\mathrm{th}} < 1.0$ and the condensate parameters (left). Absolute value of θ_{K_1} as a function of T^2 (right), which is calculated from Eq. (13), with $F_1(0)$ being fitted by Eq. (56) in the region $-10^2 < q^2 < -3\ \mathrm{GeV}^2$. The blue and red bands denote the errors from the uncertainties of the condensate parameters and $m_{K_{1A}}$, f_{1A}, $f_{1B}^{\perp}$, respectively. The purple band shows the uncertainty of τ_{th} in the region $0.6 < \tau_{\mathrm{th}} < 1.0$.

(5) using nonrelativistic constituent quark model with the inputs of the mass difference between the $a_1(1260)$ and $b_1(1235)$ mesons, as well as the ratio of the constituent quark masses [27];
(6) extracting the mixing angle from the $B \to J/\psi K_1(1270)$, $J/\psi K_1(1400)$ branching fractions by pQCD calculation;
(7) relating θ_{K_1} with a two-point correlation function, which is studied with QCDSRs [29].

It can be found that most of the $|\theta_{K_1}|$ values in the literature are in the vicinity of either 33° or 57°. Our result, $|\theta_{K_1}| = 21° \pm 9°$, is slightly below this range but consistent with that given by Ref. [26] within the error. In Ref. [26], to determine θ_{K_1}, the authors found the correspondence between θ_{K_1} and the $f_1(1285) - f_1(1420)$, $h_1(1170) - h_1(1380)$ mixing angles and ruled out unreasonable θ_{K_1} values in previous literature. In Ref. [29], a different QCDSR program was performed to extract θ_{K_1}, where the authors related θ_{K_1} with a two-point correlation function [Eq. (2) in Ref. [29]] and calculated it with OPE. However, when introducing the interpolation current of K_{1A}, the authors missed the contribution from the pseudoscalar K as illustrated in Sec. III and wrongly extracted the longitudinal component of the two-point correlation function.

TABLE I. Comparing the $|\theta_{K_1}|$ obtained in this work with those from literature.

References	$\lvert\theta_{K_1}\rvert$ (deg)
This work	21.4 ± 9 or 68.6 ± 9
(1) [22]	33 or 57
(2) [23,24]	37 or 58
(3) [25]	$(31.7^{+2.8}_{-2.5})$ or $(56.3^{+3.9}_{-4.1})$
(4) [26]	$28 < \lvert\theta_{K_1}\rvert < 30$
(5) [27]	$34 < \lvert\theta_{K_1}\rvert < 55$
(6) [28]	33 and 58
(7) [29]	39 ± 4

VI. SUMMARY

In this work, we investigate the $K_1(1270) - K_1(1400)$ mixing caused by the flavor $SU(3)$ symmetry breaking. The mixing angle is expressed by a $K_{1A} \to K_{1B}$ matrix element induced by the s quark mass operator that breaks flavor $SU(3)$ symmetry. We focus on the QCD contribution to this matrix element and calculate it with QCDSRs, where a three-point correlation function is defined and calculated both at the hadron and quark-gluon levels. In the calculation at the quark-gluon level, the operator product expansion is up to dimension-five condensates. A detailed numerical analysis is performed to determine the Borel parameters, and the obtained mixing angle is $\theta_{K_1} = 21.4° \pm 9°$ or $\theta_{K_1} = 68.6° \pm 9°$, which is consistent with the phenomenological analysis on the relation between θ_{K_1} and the mixing angle of strangeless axial-vector mesons.

ACKNOWLEDGMENTS

We thank Wei Wang and Zhen-Xing Zhao for valuable discussions. This work is supported in part by Natural Science Foundation of China under Grants No. 12305103, No. 12205180, and No. 12147140. The work of Y.-J. S. is also supported by Opening Foundation of Shanghai Key Laboratory of Particle Physics and Cosmology under Grant No. 22DZ2229013-2. The work of J. Z. is also partially supported by the project funded by China Postdoctoral Science Foundation under Grant No. 2022M712088.

APPENDIX A: TRIANGLE DIAGRAM INTEGRATION

Here we present the rank one and two triangle diagram integrations. They are defined as

$$\int d\Phi_\Delta(p_1,p_2,m_1,m_2,m)k^\mu = (A_1 p_1^\mu + B_1 p_2^\mu)I_\Delta,$$
$$\int d\Phi_\Delta(p_1,p_2,m_1,m_2,m)k^{\mu_1}k^{\mu_2} = [A_2 p_1^{\mu_1}p_1^{\mu_2} + B_2 p_2^{\mu_1}p_2^{\mu_2} + C_2(p_1^{\mu_1}p_2^{\mu_2} + p_2^{\mu_1}p_1^{\mu_2}) + D_2 g^{\mu_1\mu_2}]I_\Delta, \tag{A1}$$

where

$$A_1 = \frac{-(m^2(q^2-s_1+s_2)) + s_2(2m_1^2-q^2-s_1+s_2) + m_2^2(q^2-s_1-s_2)}{q^4-2q^2(s_1+s_2)+(s_1-s_2)^2},$$
$$B_1 = \frac{-(m^2(q^2+s_1-s_2)) + m_1^2(q^2-s_1-s_2) + s_1(2m_2^2-q^2+s_1-s_2)}{q^4-2q^2(s_1+s_2)+(s_1-s_2)^2},$$
$$A_2 = \frac{1}{(q^4+(s_1-s_2)^2-2q^2(s_1+s_2))^2}[m^4(q^4-2q^2(s_1-2s_2)+(s_1-s_2)^2)$$
$$+(6m_1^4+q^4+q^2(4s_1-2s_2)+(s_1-s_2)^2-6m_1^2(q^2+s_1-s_2))s_2^2+m_2^4(q^4+s_1^2+4s_1s_2+s_2^2-2q^2(s_1+s_2))$$
$$-2m_2^2s_2(q^4-2s_1^2+q^2(s_1-2s_2)+s_1s_2+s_2^2+3m_1^2(-q^2+s_1+s_2))$$
$$-2m^2(m_2^2(q^4+s_1^2+s_1s_2-2s_2^2+q^2(-2s_1+s_2))+s_2(-2q^4+(s_1-s_2)^2+3m_1^2(q^2-s_1+s_2)+q^2(s_1+s_2)))],$$
$$B_2 = \frac{1}{(q^4+(s_1-s_2)^2-2q^2(s_1+s_2))^2}[m^4(q^4+q^2(4s_1-2s_2)+(s_1-s_2)^2)$$
$$+s_1^2(6m_2^4+q^4-2q^2(s_1-2s_2)+(s_1-s_2)^2-6m_2^2(q^2-s_1+s_2))+m_1^4(q^4+s_1^2+4s_1s_2+s_2^2-2q^2(s_1+s_2))$$
$$-2m_1^2s_1(q^4+s_1^2+s_1s_2-2s_2^2+q^2(-2s_1+s_2)+3m_2^2(-q^2+s_1+s_2))$$
$$-2m^2(m_1^2(q^4-2s_1^2+q^2(s_1-2s_2)+s_1s_2+s_2^2)+s_1(-2q^4+(s_1-s_2)^2+3m_2^2(q^2+s_1-s_2)+q^2(s_1+s_2)))],$$
$$C_2 = \frac{1}{(q^4+(s_1-s_2)^2-2q^2(s_1+s_2))^2}[3m_1^4(q^2-s_1-s_2)s_2+m^4(2q^4-(s_1-s_2)^2-q^2(s_1+s_2))$$
$$-m^2(-q^6+q^4s_1+q^2s_1^2-s_1^3+q^4s_2-6q^2s_1s_2+s_1^2s_2+q^2s_2^2+s_1s_2^2-s_2^3$$
$$+2m_2^2(q^4+q^2s_1-2s_1^2-2q^2s_2+s_1s_2+s_2^2)+2m_1^2(q^4+s_1^2+s_1s_2-2s_2^2+q^2(-2s_1+s_2)))$$
$$+2m_1^2(-s_2(q^4-2s_1^2+q^2(s_1-2s_2)+s_1s_2+s_2^2)+m_2^2(q^4+s_1^2+4s_1s_2+s_2^2-2q^2(s_1+s_2)))$$
$$-s_1(3m_2^4(-q^2+s_1+s_2)+2m_2^2(q^4+s_1^2+s_1s_2-2s_2^2+q^2(-2s_1+s_2))$$
$$+s_2(-2q^4+(s_1-s_2)^2+q^2(s_1+s_2)))],$$
$$D_2 = \frac{1}{2(q^4+(s_1-s_2)^2-2q^2(s_1+s_2))}[m^4q^2+m_1^4s_2+m_1^2(m_2^2(q^2-s_1-s_2)$$
$$+s_2(-q^2-s_1+s_2))+s_1(m_2^4+q^2s_2-m_2^2(q^2-s_1+s_2))$$
$$-m^2(m_2^2(q^2+s_1-s_2)+m_1^2(q^2-s_1+s_2)+q^2(-q^2+s_1+s_2))]. \tag{A2}$$

APPENDIX B: ANALYTICAL RESULTS

Here we present the analytical results for the calculation of the perturbative diagram and GG condensate diagrams. The imaginary part of the correlation function contributed by the perturbative diagram reads as

$$\mathrm{Im}^2\tilde{\Pi}^{\mathrm{pert}}(p_1,p_2,q^2) = \frac{N_c}{4\pi}I_\Delta[m_s^2(2A_1+10B_1-1)+B_1(-3q^2-s_1+s_2)+s_1], \tag{B1}$$

where A_1, B_1 are taken from Eq. (A2) with $m_1=m_2=m_s$, $m=0$. The imaginary parts of the correlation function contributed by the GG condensate diagrams read as

$$\mathrm{Im}^2\tilde{\Pi}^{GG(a)}(p_1,p_2,q^2)=\frac{\langle GG\rangle}{48\pi}\frac{\partial^2}{\partial M_1^2\partial M_2^2}I_\Delta^{M_{1,2}}[M_1^2(2A_1^{M_{1,2}}+8B_1^{M_{1,2}}-1)+B_1^{M_{1,2}}(6M_2^2+24m_s^2-7q^2-s_1+s_2)+s_1]|_{M_1^2=M_2^2=m_s^2}, \tag{B2}$$

$$\begin{aligned}\mathrm{Im}^2\tilde{\Pi}^{GG(b)}(p_1,p_2,q^2)=&\frac{\langle GG\rangle}{4\pi}\frac{\partial}{\partial M_1^2}I_\Delta^{M_1}(A_1^{M_1}+B_1^{M_1}-1)|_{M_1^2=m_s^2}-\frac{\langle GG\rangle}{96((-q^2+s_1+s_2)^2-4s_1s_2)^{3/2}}\frac{\partial}{\partial M_1^2}\\
&\times[M_1^2(q^2-5s_1+5s_2)+m_s^2(q^2+s_1-s_2)+q^2(-3q^2+7s_1+3s_2)]\\
&\times\theta[(M_1^2)^2(-s_2)+M_1^2(m_s^2(-q^2+s_1+s_2)+s_2(q^2+s_1-s_2))\\
&-s_1(m_s^4-m_s^2(q^2-s_1+s_2)+q^2s_2)]\theta(s_1-M_1^2)\theta(s_2-m_s^2)|_{M_1^2=m_s^2}\\
&-\frac{\langle GG\rangle}{48((-q^2+s_1+s_2)^2-4s_1s_2)^{3/2}}\frac{\partial}{\partial M_1^2}[(M_1^2)^2s_2+M_1^2(q^2-s_1-s_2)(m_s^2-q^2+s_1-s_2)\\
&+m_s^4s_1-2m_s^2(q^4-q^2(s_1+2s_2)+s_2(s_2-s_1))+q^2(q^4-2q^2(s_1+s_2)+s_1^2+s1s_2+s_2^2)]\\
&\times\frac{s_{2,M_1}^{(2)}-s_{2,M_1}^{(1)}}{|s_{2,M_1}^{(2)}-s_{2,M_1}^{(1)}|}[\delta(s_2-s_{2,M_1}^{(1)})-\delta(s_2-s_{2,M_1}^{(2)})]|_{M_1^2=m_s^2}-\frac{\langle GG\rangle}{48((-q^2+s_1+s_2)^2-4s_1s_2)^{3/2}}\frac{\partial}{\partial M_1^2}\\
&\times[s_1(M_1^2(q^2-s_1+s_2)+m_s^2(q^2+s_1-s_2)+q^2(-q^2+s_1+s_2))]\\
&\times\frac{s_{1,M_1}^{(2)}-s_{1,M_1}^{(1)}}{|s_{1,M_1}^{(2)}-s_{1,M_1}^{(1)}|}[\delta(s_1-s_{1,M_1}^{(1)})-\delta(s_1-s_{1,M_1}^{(2)})]|_{M_1^2=m_s^2},\end{aligned} \tag{B3}$$

$$\begin{aligned}\mathrm{Im}^2\tilde{\Pi}^{GG(c)}(p_1,p_2,q^2)=&\frac{\langle GG\rangle}{8\pi}\frac{\partial}{\partial M_2^2}I_\Delta^{M_2}(A_1^{M_2}+B_1^{M_2}-1)|_{M_2^2=m_s^2}-\frac{\langle GG\rangle}{48((-q^2+s_1+s_2)^2-4s_1s_2)^{3/2}}\frac{\partial}{\partial M_2^2}\\
&\times[3M_2^2(q^2+s_1-s_2)-m_s^2(q^2+7s_1-7s_2)+q^2(-3q^2+7s_1+3s_2)]\theta[-(M_2^2)^2s_1\\
&+m_s^2(M_2^2(-q^2+s_1+s_2)+s_2(q^2+s_1-s_2))+M_2^2s_1(q^2-s_1+s_2)\\
&+m_s^4(-s_2)-q^2s_1s_2]\theta(s_1-m_s^2)\theta(s_2-M_2^2)|_{M_2^2=m_s^2}-\frac{\langle GG\rangle}{24((-q^2+s_1+s_2)^2-4s_1s_2)^{3/2}}\frac{\partial}{\partial M_2^2}\\
&\times[(M_2^2)^2s_1+M_2^2(q^2-s_1-s_2)(m_s^2-q^2-s_1+s_2)+m_s^4s_2\\
&-2m_s^2(q^4-q^2(2s_1+s_2)+s_1(s_1-s_2))+q^2(q^4-2q^2(s_1+s_2)+s_1^2+s_1s_2+s_2^2)]\\
&\times\frac{s_{2,M_2}^{(2)}-s_{2,M_2}^{(1)}}{\left|s_{2,M_2}^{(2)}-s_{2,M_2}^{(1)}\right|}[\delta(s_2-s_{2,M_2}^{(1)})-\delta(s_2-s_{2,M_2}^{(2)})]|_{M_2^2=m_s^2}-\frac{\langle GG\rangle}{24((-q^2+s_1+s_2)^2-4s_1s_2)^{3/2}}\frac{\partial}{\partial M_2^2}\\
&\times[M_2^2(q^2+s_1-s_2)+m_s^2(q^2-s_1+s_2)+q^2(-q^2+s_1+s_2)]\\
&\times\frac{s_{1,M_2}^{(2)}-s_{1,M_2}^{(1)}}{|s_{1,M_2}^{(2)}-s_{1,M_2}^{(1)}|}[\delta(s_1-s_{1,M_2}^{(1)})-\delta(s_1-s_{1,M_2}^{(2)})]|_{M_2^2=m_s^2},\end{aligned} \tag{B4}$$

where

$$\begin{aligned}(I_\Delta^{M_{1,2}},A_1^{M_{1,2}},B_1^{M_{1,2}})&=(I_\Delta,A_1,B_1)|_{m_1=M_1,m_2=M_2,m=0},\\
(I_\Delta^{M_1},A_1^{M_1},B_1^{M_1})&=(I_\Delta,A_1,B_1)|_{m_1=M_1,m_2=m_s,m=0},\\
(I_\Delta^{M_2},A_1^{M_2},B_1^{M_2})&=(I_\Delta,A_1,B_1)|_{m_1=m_s,m_2=M_2,m=0},\\
s_{i,M_1}^{(j)}&=s_i^{(j)}|_{m_1=M_1,m_2=m_s},\\
s_{i,M_2}^{(j)}&=s_i^{(j)}|_{m_1=m_s,m_2=M_2},\end{aligned} \tag{B5}$$

with $s_i^{(j)}$ defined as

$$
\begin{aligned}
s_1^{(1)} &= \frac{m_1^2(m_2^2+s_2)+(m_2^2-s_2)(\sqrt{m_1^4-2m_1^2(m_2^2+q^2)+(m_2^2-q^2)^2}-m_2^2+q^2)}{2m_2^2},\\
s_1^{(2)} &= \frac{m_1^2(m_2^2+s_2)-(m_2^2-s_2)(\sqrt{m_1^4-2m_1^2(m_2^2+q^2)+(m_2^2-q^2)^2}+m_2^2-q^2)}{2m_2^2},\\
s_2^{(1)} &= -\frac{m_1^4-m_1^2m_2^2-m_1^2q^2-m_1^2s_1+(s_1-m_1^2)\sqrt{m_1^4-2m_1^2(m_2^2+q^2)+(m_2^2-q^2)^2}-m_2^2s_1+q^2s_1}{2m_1^2},\\
s_2^{(2)} &= -\frac{m_1^4-m_1^2m_2^2-m_1^2q^2-m_1^2s_1+(m_1^2-s_1)\sqrt{m_1^4-2m_1^2(m_2^2+q^2)+(m_2^2-q^2)^2}-m_2^2s_1+q^2s_1}{2m_1^2}.
\end{aligned} \tag{B6}
$$

It should be noted that, for the $GG(a)$ diagram, before doing derivatives on M_1^2 and M_2^2, the masses of the k_1, k_2, k lines are set as $M_1, M_2, 0$. For the $GG(b)$ and $GG(c)$ diagrams, before doing derivatives, the masses of the k_1, k_2, k lines are set as $M_1, m_s, 0$ and $m_s, M_2, 0$, respectively.

Finally, we take Fig. 4(e) as an example to illustrate why the amplitudes of this diagram as well as Figs. 4(d) and 4(f) are suppressed. The amplitude of Fig. 4(e) reads as

$$
\begin{aligned}
\Pi_{\mu\nu\rho}^{GG(e)}(p_1,p_2,q^2) &= \int d^4x d^4y e^{ip_2\cdot x}e^{-ip_1\cdot y}\int\frac{d^4k_1}{(2\pi)^4}\frac{d^4k_2}{(2\pi)^4}\frac{d^4k}{(2\pi)^4}e^{ik_1\cdot y}e^{-ik_2\cdot x}e^{-ik\cdot(y-x)}\left(-\frac{i}{4}\right)\\
&\times \mathrm{tr}\left[\frac{-i\not{k}}{k^2}\sigma_{\mu\nu}\frac{i\not{k}_2}{k_2^2-m_s^2}\frac{[f^{\alpha\beta\kappa\tau}(k_1)+f^{\alpha\kappa\beta\tau}(k_1)+f^{\alpha\kappa\tau\beta}(k_1)]}{(k^2-m_s^2)^2}\gamma_\rho\gamma_5\right]\\
&\times \mathrm{tr}[t^At^A]g_s^2\langle 0|G_{\alpha\beta}^A(0)G_{\kappa\tau}^A(0)|0\rangle.
\end{aligned} \tag{B7}
$$

Calculating the complex trace as shown above and performing the projection defined in Eq. (19), one can obtain an expression proportional to m_s^2. Accordingly, the imaginary part is

$$
\begin{aligned}
\mathrm{Im}^2\tilde{\Pi}^{GG(e)}(p_1,p_2,q^2) &= m_s^2\frac{\langle GG\rangle}{16\pi}\frac{\partial}{\partial M_1^2}I_\Delta(M_1^2-m_s^2)[M_1^2(2A_1^{M_1}+8B_1^{M_1}-1)\\
&+B_1^{M_1}(2m_s^2-3q^2-s_1+s_2)+s_1]|_{M_1^2=m_s^2},
\end{aligned} \tag{B8}
$$

which is proportional to m_s^2. Therefore, compared with the amplitudes of Figs. 4(a)–4(c) and 4(e) is $\mathcal{O}(m_s^2)$ suppressed so that it can be neglected. The same reason also enables us to neglect Figs. 4(d) and 4(f).

[1] D. Zeppenfeld, SU(3) relations for B meson decays, Z. Phys. C **8**, 77 (1981).
[2] M. J. Savage and M. B. Wise, SU(3) predictions for non-leptonic B meson decays, Phys. Rev. D **39**, 3346 (1989); **40**, 3127(E) (1989).
[3] N. G. Deshpande and X. G. He, CP Asymmetry Relations Between $\bar{B}^0\to\pi\pi$ and $\bar{B}^0\to\pi K$ rates, Phys. Rev. Lett. **75**, 1703 (1995).
[4] L. L. Chau and H. Y. Cheng, Quark Diagram Analysis of Two-body Charm Decays, Phys. Rev. Lett. **56**, 1655 (1986).
[5] L. L. Chau, H. Y. Cheng, W. K. Sze, H. Yao, and B. Tseng, Charmless nonleptonic rare decays of B mesons, Phys. Rev. D **43**, 2176 (1991); **58**, 019902(E) (1998).
[6] C. D. Lü, W. Wang, and F. S. Yu, Test flavor SU(3) symmetry in exclusive Λ_c decays, Phys. Rev. D **93**, 056008 (2016).
[7] W. Wang, Z. P. Xing, and J. Xu, Weak decays of doubly heavy baryons: SU(3) analysis, Eur. Phys. J. C **77**, 800 (2017).
[8] X. G. He and W. Wang, Flavor SU(3) topological diagram and irreducible representation amplitudes for heavy meson charmless hadronic decays: Mismatch and equivalence, Chin. Phys. C **42**, 103108 (2018).
[9] H. Hatanaka and K. C. Yang, $B\to K_1\gamma$ decays in the light-cone qcd sum rules, Phys. Rev. D **77**, 094023 (2008); **78**, 059902(E) (2008).

[10] A. Sikandar, M. J. Aslam, I. Ahmed, and S. Shafaq, Radiative B to axial-vector meson decays at NLO in soft-collinear effective theory, J. Phys. G **48**, 045005 (2021).
[11] A. Bhatta and R. Mohanta, Implications of new physics in $B \to K_1 \mu^+ \mu^-$ decay processes, J. Phys. G **48**, 085011 (2021).
[12] F. Munir Bhutta, Z. R. Huang, C. D. Lü, M. A. Paracha, and W. Wang, New physics in $b \to s l^+ l^-$ anomalies and its implications for the complementary neutral current decays, Nucl. Phys. **B979**, 115763 (2022).
[13] Z. R. Huang, M. A. Paracha, I. Ahmed, and C. D. Lü, Testing leptoquark and Z' models via $B \to K_1(1270, 1400)\mu^+\mu^-$ decays, Phys. Rev. D **100**, 055038 (2019).
[14] S. Momeni and R. Khosravi, Analysis of the semileptonic $B \to K_1 \ell^+ \ell^-$transitions and non-leptonic $B \to K_1 \gamma$ decay in the AdS/QCD correspondence, Eur. Phys. J. C **78**, 805 (2018).
[15] N. Ahmed, I. Ahmed, and M. J. Aslam, Analysis of forward–backward and lepton polarization asymmetries in $B \to K_1 \ell^+ \ell^-$ decays in the two-Higgs-doublet model, Prog. Theor. Exp. Phys. **2015**, 113B06 (2015).
[16] F. Falahati and A. Zahedidareshouri, Forward-backward asymmetries of $\bar{B} \to \bar{K}_1(1270)\ell^+\ell^-$ and $\bar{B} \to \bar{K}^* \ell^+ \ell^-$ transitions in two Higgs doublet model, Phys. Rev. D **90**, 075002 (2014).
[17] Y. Li, J. Hua, and K. C. Yang, $B \to K_1 \ell^+ \ell^-$ decays in a family non-universal Z' model, Eur. Phys. J. C **71**, 1775 (2011).
[18] E. Kou, A. Le Yaouanc, and A. Tayduganov, Determining the photon polarization of the $b \to s\gamma$ using the $B \to K_1(1270)\gamma \to (K\pi\pi)\gamma$ decay, Phys. Rev. D **83**, 094007 (2011).
[19] W. Wang, F. S. Yu, and Z. X. Zhao, Novel method to reliably determine the photon helicity in $B \to K_1 \gamma$, Phys. Rev. Lett. **125**, 051802 (2020).
[20] P. F. Guo, D. Wang, and F. S. Yu, Strange axial-vector mesons in D meson decays, Nucl. Phys. Rev. **36**, 125 (2019).
[21] V. Shastry, E. Trotti, and F. Giacosa, Constraints imposed by the partial wave amplitudes on the decays of $J = 1, 2$ mesons, Phys. Rev. D **105**, 054022 (2022).
[22] M. Suzuki, , Strange axial-vector mesons, Phys. Rev. D **47**, 1252 (1993).
[23] H. Y. Cheng, Hadronic charmed meson decays involving axial vector mesons, Phys. Rev. D **67**, 094007 (2003).
[24] R. H. Li, C. D. Lu, and W. Wang, Transition form factors of B decays into p-wave axial-vector mesons in the perturbative QCD approach, Phys. Rev. D **79**, 034014 (2009).
[25] F. E. Close and A. Kirk, Implications of the glueball $-\bar{q}q$ filter on the 1^{++} nonet, Z. Phys. C **76**, 469 (1997).
[26] H. Y. Cheng, Mixing angle of K_1 axial vector mesons, *Proc. Sci.*, Hadron2013 (2013) 090 [arXiv:1311.2370].
[27] L. Burakovsky and J. T. Goldman, Constraint on axial-vector meson mixing angle from nonrelativistic constituent quark model, Phys. Rev. D **56**, R1368 (1997).
[28] Z. Q. Zhang, H. Guo, and S. Y. Wang, Study of the $K_1(1270) - K_1(1400)$ mixing in the decays $B \to J/\Psi K_1(1270), J/\Psi K_1(1400)$, Eur. Phys. J. C **78**, 219 (2018).
[29] H. Dag, A. Ozpineci, A. Cagil, and G. Erkol, Theoretical determination of K(1)(1270,1400) mixing angle in QCD, J. Phys. Conf. Ser. **348**, 012012 (2012).
[30] H. Liu, L. Liu, P. Sun, W. Sun, J. X. Tan, W. Wang, Y. B. Yang, and Q. A. Zhang, $\Xi_c - \Xi_c{}'$ mixing from lattice QCD, Phys. Lett. B **841**, 137941 (2023).
[31] Z. F. Deng, Y. J. Shi, W. Wang, and J. Zeng, QED contributions to the $\Xi_c - \Xi_c{}'$ mixing, arXiv:2309.16386.
[32] A. I. Onishchenko, Exclusive decays of Xi(QQ') baryons in NRQCD sum rules, arXiv:hep-ph/0006271.
[33] A. I. Onishchenko, Inclusive and exclusive decays of doubly heavy baryons, arXiv:hep-ph/0006295.
[34] V. V. Kiselev and A. K. Likhoded, Baryons with two heavy quarks, Phys. Usp. **45**, 455 (2002).
[35] J. R. Zhang and M. Q. Huang, Doubly heavy baryons in QCD sum rules, Phys. Rev. D **78**, 094007 (2008).
[36] Z. G. Wang, Analysis of the $\frac{1}{2}^+$ doubly heavy baryon states with QCD sum rules, Eur. Phys. J. A **45**, 267 (2010).
[37] Z. G. Wang, Analysis of the $\frac{3}{2}^+$ heavy and doubly heavy baryon states with QCD sum rules, Eur. Phys. J. C **68**, 459 (2010).
[38] Z. G. Wang, Analysis of the $1/2^-$ and $3/2^-$ heavy and doubly heavy baryon states with QCD sum rules, Eur. Phys. J. A **47**, 81 (2011).
[39] X. H. Hu, Y. L. Shen, W. Wang, and Z. X. Zhao, Weak decays of doubly heavy baryons: "decay constants”, Chin. Phys. C **42**, 123102 (2018).
[40] Y. J. Shi, W. Wang, and Z. X. Zhao, QCD sum rules analysis of weak decays of doubly-heavy baryons, Eur. Phys. J. C **80**, 568 (2020).
[41] V. A. Novikov, M. A. Shifman, A. I. Vainshtein, and V. I. Zakharov, Calculations in external fields in quantum chromodynamics. Technical review, Fortschr. Phys. **32**, 585 (1984).
[42] K. C. Yang, Light-cone distribution amplitudes of axial-vector mesons, Nucl. Phys. **B776**, 187 (2007).
[43] P. A. Zyla *et al.* (Particle Data Group), Review of particle physics, Prog. Theor. Exp. Phys. **2020**, 083C01 (2020).
[44] B. L. Ioffe, QCD at low energies, Prog. Part. Nucl. Phys. **56**, 232 (2006).
[45] P. Colangelo and A. Khodjamirian, QCD sum rules, a modern perspective, *At The Frontier of Particle Physics* (World Scientific, Singapore, 2001).